analytical chemistry

Feature

pubs.acs.org/ac

Unraveling the Mechanism of Electrospray Ionization

Electrospray ionization (ESI) generates intact gas-phase ions from analytes in solution for mass spectrometric investigations. ESI can proceed via different mechanisms. Low molecular weight analytes follow the ion evaporation model (IEM), whereas the charged residue model (CRM) applies to large globular species. A chain ejection model (CEM) has been proposed for disordered polymers.

Lars Konermann,* Elias Ahadi, Antony D. Rodriguez, and Siavash Vahidi

Department of Chemistry, The University of Western Ontario, London, Ontario, N6A 5B7 Canada

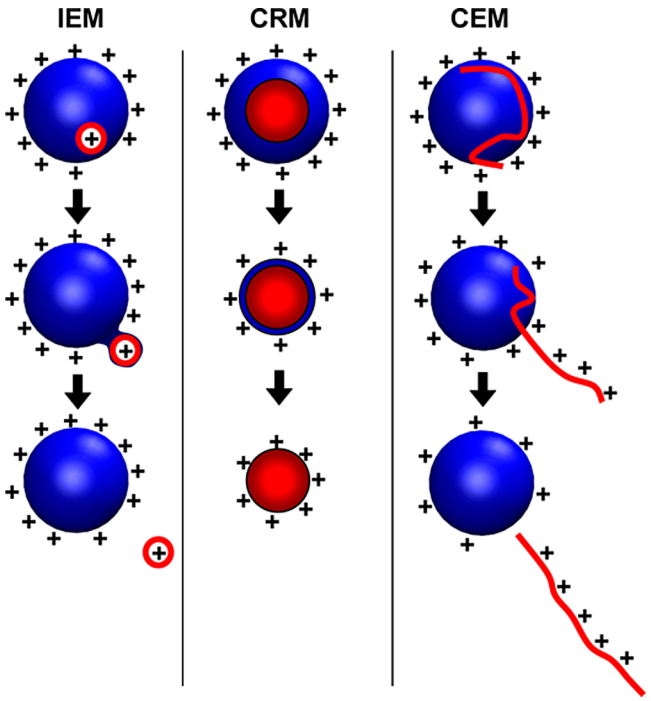

Mass spectrometry (MS) is among the most widely used analytical techniques. Every mass spectrometer comprises an analyzer that measures the mass-to-charge ratio (m/z) of chemical species (i) that are present in gaseous form and (ii) that carry a net charge. Most molecules of interest are condensed-phase species that may or may not be charged. Converting these analytes into gaseous ions is a key prerequisite for MS experiments.

MS has been revolutionized over the past two decades, as electrospray ionization (ESI)[1] and matrix-assisted laser desorption/ionization (MALDI)[2] became widely available. These ionization techniques enable investigations on a wide variety of compounds, all the way to the MDa range.[3,4] For MALDI, analytes are embedded in a solid matrix, and gaseous ions are formed by exposure to a laser pulse.[5] In contrast, ESI converts solution-phase analytes into gas-phase ions.[1,6] ESI and MALDI are "soft" ionization techniques; i.e., they induce little or no fragmentation. This is in contrast to electron impact (EI) and other traditional approaches, where the rupture of covalent bonds is commonplace.

Both ESI and MALDI can generate $[M + zH]^{z+}$ ions. It is quite common for MALDI to form singly charged species ($z = 1$), whereas multiple charging ($z \gg 1$) is the norm for ESI. Multiple charging can be beneficial, e.g., it allows the detection of large analytes on mass spectrometers with limited m/z range. Also, high charge states facilitate ion dissociation in tandem MS experiments. Possibly, the most important advantage of ESI is the straightforward coupling with liquid chromatography (LC) for the online separation of complex mixtures prior to MS. Proteomic digests represent one example where LC/ESI-MS has had a major impact.[7] The close linkage between solution-phase chemistry and gas-phase detection in ESI-MS also facilitates other applications such as hydrogen/deuterium exchange measurements,[8] protein−ligand binding experiments,[3,9] and enzyme kinetic investigations.[10] The low m/z range in MALDI-MS tends to be obscured by chemical noise. This problem is less pronounced in LC/ESI-MS, thus facilitating the analysis of low molecular weight (MW) species such as drugs and metabolites.

Analytical chemists generally strive to develop a complete mechanistic understanding of the tools that are at their disposal. Knowledge gaps may lead to improperly designed experiments or to erroneous data interpretation. Uncovering the intricacies of the ESI process has proven to be surprisingly difficult and remains an active area of research.[11,12] Although some aspects have been thoroughly explored,[6,13−15] "there is still much debate on the mechanism(s) by which...gaseous ions are formed" (quoted from a 2007 paper of ESI-MS developer and Nobel Prize winner John Fenn).[16] In recent years, molecular dynamics (MD) simulations have yielded new insights into this area.[17−24] MD simulations are based on the iterative integration of Newton's Laws, thus providing molecular movies of physical/chemical phenomena. The purpose of this Feature is to provide an overview of the current understanding of the ESI process. We primarily focus on the final steps, which represent the most elusive regime.

FROM ANALYTE SOLUTION TO HIGHLY CHARGED NANODROPLETS

The basic operation principles of ESI sources have been discussed in several excellent reviews (see, e.g., refs 1, 6, 14, 15 and 25). We will briefly summarize the salient points to facilitate the understanding of subsequent sections.

ESI occurs at atmospheric pressure.[26] Analyte solution is infused into a metal capillary that is held at an electric potential of several kV (Figure 1). We will limit our discussion to the

Published: November 7, 2012

   dx.doi.org/10.1021/ac302789c | *Anal. Chem.* 2013, 85, 2−9

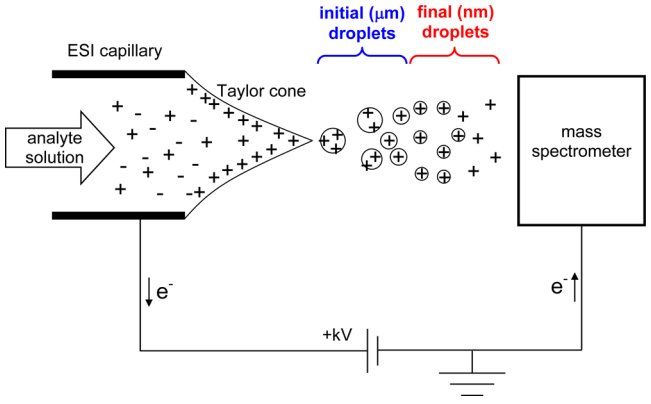

Figure 1. Schematic depiction of an ESI source operated in positive ion mode.

commonly used positive ion mode, where the potential is positive vs ground. Typical infusion rates are between one and several hundred μL min^{-1}, well compatible with LC. The solution at the capillary tip is distorted into a Taylor cone that emits a fine mist of droplets.[27] This spraying process is usually assisted by a coaxial gas flow (not shown in Figure 1).[26] The initial ESI droplets have radii in the micrometer range. Each droplet is positively charged due to the presence of excess ions that can include H^+, NH_4^+, Na^+, and K^+. Protons are often the main contributor to the net droplet charge, partly because many analyte solutions are acidic. More importantly, protons are generated at the metal/solution interface inside the capillary (e.g., 2 $H_2O \rightarrow 4\ H^+ + 4\ e^- + O_2$).[15] Due to the occurrence of these and other charge-balancing reactions, the ESI source represents an electrochemical cell.[28] The current in the circuit of Figure 1 is mediated by ions and charged droplets that move in the gas phase, as well as electron flow through the wires that connect the ESI capillary (anode) to the mass spectrometer (cathode).[15]

The droplets emitted from the Taylor cone undergo rapid solvent evaporation, often assisted by heating. In the case of aqueous/organic mixtures, the organic component usually evaporates more readily, causing a gradual increase in water percentage.[6,18,29] The charge density on the shrinking droplets builds up until surface tension is balanced by Coulombic repulsion. At this so-called Rayleigh limit, the number z_R of elementary charges e is given by[30]

$$z_R = \frac{8\pi}{e}\sqrt{\varepsilon_0 \gamma R^3} \quad (1)$$

where R is the droplet radius, ε_0 is the vacuum permittivity, and γ is the surface tension. Droplets at the Rayleigh limit produce even smaller and highly charged offspring droplets via jet fission. Repeated evaporation/fission events ultimately yield the final generation of ESI droplets with radii of a few nanometers. *Gaseous analyte ions that are detected by MS are produced from these highly charged nanodroplets.*[1,6,14,16] Three different ion release mechanisms (IEM, CRM, and CEM) will be discussed below.

NanoESI represents a variation of the ESI theme. It employs emitter tip openings of only a few μm, instead of ~100 μm for conventional ESI. NanoESI operates at flow rates down to <10 nL min^{-1}. Attributes of nanoESI include reduced sample consumption, increased sensitivity, and enhanced ionization efficiency.[26,31,32] Due to their narrow opening, nanoESI emitters are prone to clogging. Array emitters can help mitigate this problem.[33] Claims that nanoESI is even "softer" than conventional ESI are not necessarily confirmed by experiments.[34] The small nozzle diameter in nanoESI reduces the size of the initially produced droplets. As a result, a lower number of evaporation/fission cycles is required before analyte ions are released into the gas phase. It is emphasized that highly charged nanodroplets are the precursors of gaseous analyte ions in both conventional ESI and nanoESI.[6] The following sections will therefore not distinguish between the two variants.

LOCATION OF CHARGE IN ESI NANODROPLETS

Gauss' Law dictates that electric charge on an isolated conductor moves entirely to the outer surface.[35] ESI investigations, therefore, often assume that all excess ions are located directly at the surface of the droplet.[1,6,14,16] On the other hand, ion positions at the surface should be unfavorable due to partial loss of solvation. It is interesting how these conflicting trends are reconciled.

MD simulations were used to explore the behavior of Na^+-containing water nanodroplets close to the Rayleigh limit (1250 H_2O molecules and 10 Na^+, $R \approx 2.1$ nm, Figure 2a).[17] It was found that the ions prefer positions in the droplet interior where they are well solvated. Surprisingly, the net charge is nonetheless located on the droplet surface. This apparent

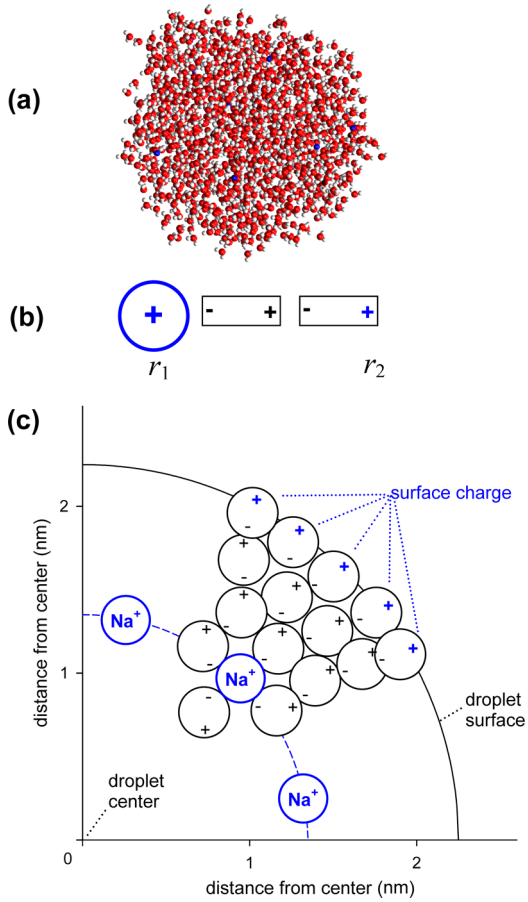

Figure 2. (a) Snapshot of an MD-generated water nanodroplet containing 10 excess sodium ions (blue: Na^+; red: O; white: H). (b) Cartoon illustration of an ion that interacts with two oriented dipoles. (c) Schematic representation, illustrating the internal positioning of Na^+ and water dipoles within a nanodroplet. Reprinted from ref 17. Copyright 2010 American Chemical Society.

dx.doi.org/10.1021/ac302789c | *Anal. Chem.* 2013, 85, 2–9

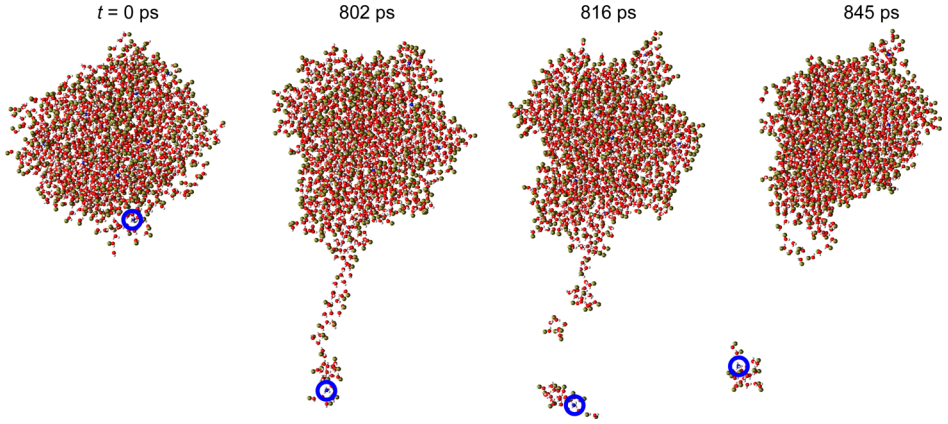

Figure 3. Snapshots from a MD simulation of a Rayleigh-charged nanodroplet containing 750 water molecules, 750 methanol molecules, and 11 NH_4^+. Color coding is as in Figure 2, with $-CH_3$ shown in ochre. The NH_4^+ ion that is being emitted is highlighted by a blue circle. Reprinted from ref 18. Copyright 2011 American Chemical Society.

paradox is resolved when considering how a dipolar solvent interacts with charged moieties. Figure 2b illustrates a hypothetical arrangement where a cation is located at position r_1, in contact with two oriented dipoles. The dipoles neutralize a fraction of the ionic charge at site r_1, effectively transferring it to r_2. A similar situation applies to charged nanodroplets (Figure 2c). The ions within the droplet induce large-scale orientational polarization of the surrounding water. This solvation arrangement projects the excess charge to the surface.[17] The observed behavior confirms the validity of Gauss' Law.[35] At the same time, the solvation requirements of all ions are satisfied. It is noted that the charge carrier location within the droplet will depend on the type of ion. Na^+ prefers positions in the interior because it tends to be strongly solvated (Figure 2).[17] Species that carry nonpolar moieties (e.g., alkylated ammonium ions)[14] will adopt positions closer to the droplet periphery.

In summary, excess charge is located on the droplet surface, while excess ions can reside in the interior. The two things are not necessarily identical. For the droplet in Figure 2, the ten Na^+ define the overall net charge of the droplet, whereas the surface charge is constituted by the positive ends of water dipoles in the outermost solvent layer. In a similar fashion, any excess ionic charge residing in the droplet interior will be projected to the surface.[35]

EJECTION OF LOW MW SPECIES INTO THE GAS PHASE: THE IEM

Low MW species that exist as preformed solution-phase ions are thought to be transferred into the gas phase via the ion evaporation model (IEM).[36] The analyte charge typically results from protonation, often assisted by an organic acid in the solution. Small inorganic ions are subject to the IEM as well. The IEM is based on the fact that the electric field emanating from a Rayleigh-charged nanodroplet (with $R < 10$ nm) is sufficiently high to cause the ejection of small solvated ions from the droplet surface. Transition state theory can be used to express the ejection rate constant k as[6,36,37]

$$k = \frac{k_B T}{h} \exp\left(\frac{-\Delta G^*}{k_B T}\right) \quad (2)$$

where ΔG^* is the height of the activation free energy barrier, k_B is the Boltzmann constant, h is Planck's constant, and T is the temperature. Originally, it was envisioned that the activation barrier arises from the opposing forces experienced by a solvated ion that has just left a perfectly spherical droplet: (i) Solvent polarization creates an image charge that tends to pull the ion back into the droplet. (ii) Repulsion by the excess droplet charge tends to push the ion further away from the droplet. MD simulations have modified this picture somewhat. The departing ion initially remains connected to the droplet by a "sticky" string of solvent molecules.[18] Figure 3 illustrates how a solvated ammonium ion is ejected from a water/methanol droplet. An extended solvent bridge is formed, which then ruptures as the solvated ion is released. This bridging phenomenon is somewhat less pronounced for droplets that are purely aqueous, in line with the higher surface tension of water.[18] The primary IEM product is a small gas-phase cluster, consisting of the ion and a few solvent molecules. This residual solvation shell is lost as the cluster travels through the sampling interface of the mass spectrometer, where it experiences collisions with background gas.[21]

There are morphological parallels between the IEM (Figure 3)[18] and Rayleigh fission events that occur for larger droplets.[38] An IEM-ejected ion with its solvation shell can be interpreted as a (very small) offspring droplet. Thus, the classical[36] dividing line between ion ejection and droplet fission becomes somewhat blurred in the nanoregime.

Figure 4 takes a closer look at the ion dynamics under IEM conditions. The free energy profile experienced by NH_4^+ in a Rayleigh-charged water droplet is depicted in Figure 4a. This profile emphasizes the metastable nature of the ion/droplet system, with a local free energy minimum located at ca. 70% of the droplet radius. The ions undergo diffusive motions, preferentially sampling radial positions close to this local minimum (Figure 4b, trajectories 1, 2). IEM ejection requires ions to cross an activation barrier of ~32 kJ mol^{-1}. Trajectory 3 represents a failed barrier crossing attempt. In contrast, trajectory 4 illustrates a successful IEM event, culminating in the ejection of a solvated ammonium ion.[18] It is seen from these data that IEM events occur on a time scale of ~1 ns. A behavior similar to that illustrated here for NH_4^+ is believed to be responsible for low MW analytes, such as protonated drugs and metabolites.[18] A cartoon summary of the IEM is provided in Figure 5a.

Analyte ions carrying nonpolar moieties usually exhibit a very strong ESI-MS response. This effect can be attributed to the

dx.doi.org/10.1021/ac302789c | Anal. Chem. 2013, 85, 2–9

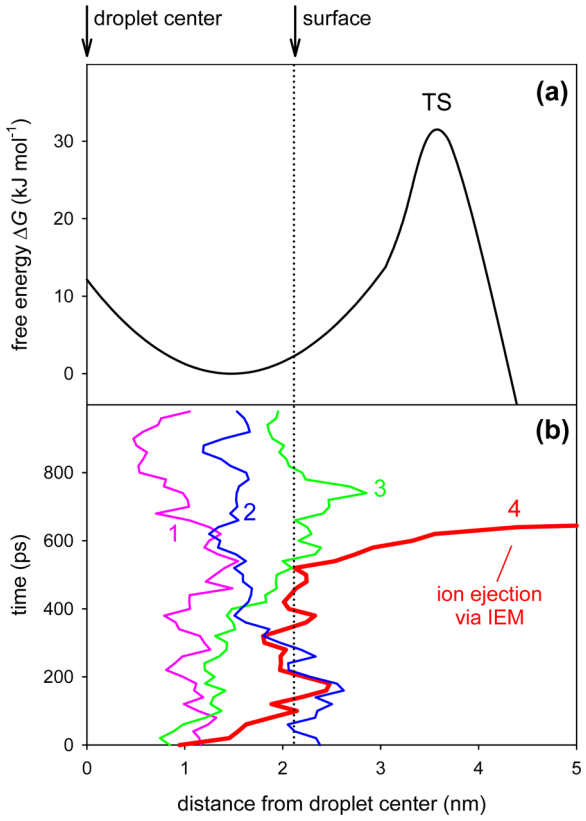

Figure 4. NH_4^+ dynamics within a Rayleigh-charged water droplet ($R \approx 2.1$ nm) under IEM conditions. (a) Free energy profile experienced by the ions. "TS" indicates the transition state. (b) Radial position of four selected ions (1–4) vs time. Ion 4 gets ejected via the IEM. Reprinted from ref 18. Copyright 2011 American Chemical Society.

fact that these species prefer positions close to the droplet surface (discussed above).[14] Offspring droplets are always formed from the outermost layers of their parent droplet. Thus, the final nanodroplets that release gaseous ions are enriched in species with the highest surface affinity. In addition, positioning of analytes close to the liquid–vapor interface will generally facilitate IEM ejection.

TRANSFERRING LARGE, GLOBULAR ANALYTES INTO THE GAS PHASE: THE CRM

It is widely accepted that large globular species such as natively folded proteins are released into the gas phase via the charged residue model (CRM, Figure 5b).[6,39,40] For the CRM, Rayleigh-charged nanodroplets that contain a single analyte evaporate to dryness. As the last solvent shell disappears, the charge of the vanishing droplet is transferred to the analyte.[6,39] CRM nanodroplets remain close to the Rayleigh limit throughout the entire shrinkage process (Figure 5b top and middle panels), implying that the droplet sheds charge as its radius decreases. This charge reduction can take place by IEM ejection of solvated protons and small ions.[12]

Direct MD simulations of the complete CRM progression are complicated by the relatively long (μs) time scale of the events. Computational studies have confirmed, however, that extensive hydration of the protein exterior traps the globular analyte deep within the droplet.[19,22,23] This behavior is consistent with the CRM. IEM ejection of the folded protein is not kinetically viable. Strong experimental support for the CRM comes from the observation that ESI of globular proteins produces ions with a composition close to $[M + z_R\,H]^{z_R+}$, where z_R is the Rayleigh charge of protein-sized water droplets (eq 1).[3,6,13,41]

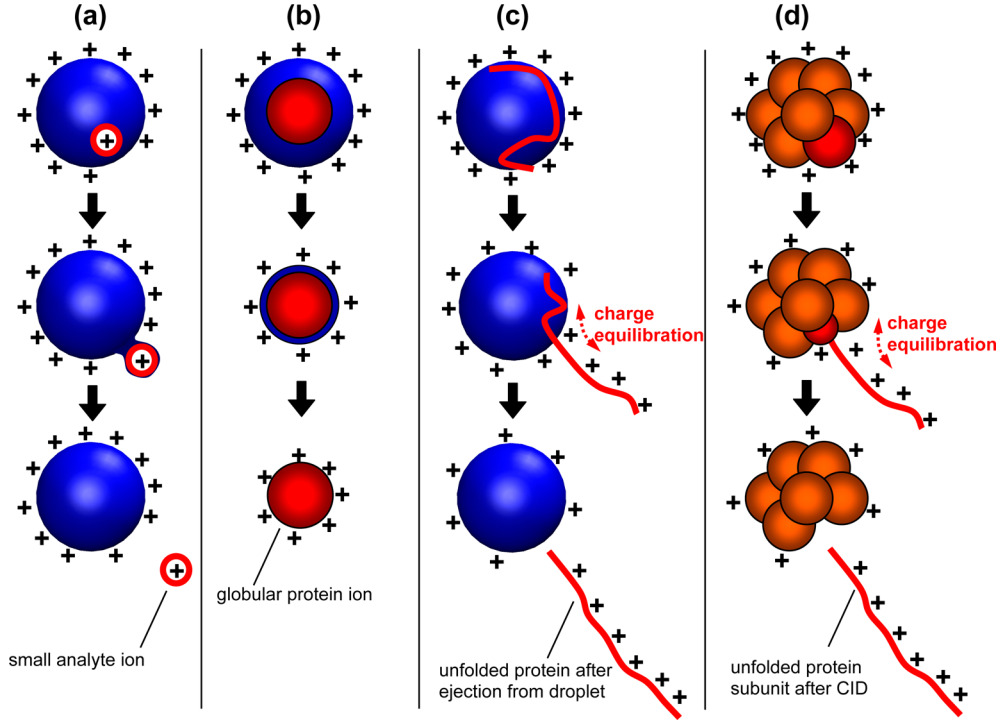

Figure 5. Summary of ESI mechanisms. (a) IEM: Small ion ejection from a charged nanodroplet. (b) CRM: Release of a globular protein into the gas phase. (c) CEM: Ejection of an unfolded protein. (d) Collision-induced dissociation of a gaseous multiprotein complex. Charge equilibration in panels c and d is indicated by red arrows. Reprinted from ref 47. Copyright 2012 American Chemical Society.

dx.doi.org/10.1021/ac302789c | *Anal. Chem.* 2013, 85, 2–9

Consistent with experimental observations,[3,6,13,41] the ESI protonation state predicted by the CRM (eq 1) does not depend on the analyte charge in solution. To rationalize this somewhat surprising[42] behavior, we will first consider a hypothetical globular protein that carries 20 positive (Arg, Lys) and 20 negative (Asp, Glu) side chains, for an overall charge of zero. Now the protein is placed within a nanodroplet that is Rayleigh-charged due to excess H^+. Solvent evaporation occurs until the droplet is barely larger than the protein. The z_R excess protons on the vanishing droplet will then bind to $-COO^-$ groups on the protein surface. The charge of the gaseous protein ion formed in this way is $(+20) + (-20) + z_R = z_R$.

Let us now consider a protein that carries a solution-phase charge of +5, resulting from 20 positive and 15 negative side chains.[42] All other parameters are the same as above. When placed into a Rayleigh-charged droplet, the protein net charge of +5 is projected to the droplet surface (analogous to the mechanism of Figure 2). In this scenario, excess protons on the droplet and the net charge of the protein contribute to the droplet's Rayleigh charge. As a result, the number of excess H^+ on the vanishing droplet is reduced to $(z_R - 5)$. H^+ binding by $-COO^-$ groups results in a gaseous protein with a net charge of $(+20) + (-15) + (z_R - 5) = z_R$, identical to the previous example. These considerations make it clear why the CRM can predict the ESI protonation state of globular proteins via eq 1, regardless of intrinsic protein charge or amino acid composition.[41]

SPECTRAL NOISE AND NONSPECIFIC ADDUCTS

ESI-MS is susceptible to signal degradation caused by the presence of solvent additives and contaminants. We will focus on the case of protein spectra recorded under physiological conditions (aqueous solution at pH ≈ 7), where this issue can be particularly pronounced. The CRM readily explains some of the challenges encountered in these experiments.

Clean $[M + z_RH]^{z_R+}$ protein ions can be formed via the CRM under conditions where the excess charge of the droplet is predominantly due to protons. In the presence of other charge carriers such as Na^+, the CRM generates a mixture of $[M + (z_R - i)H + iNa]^{z_R+}$ ions, where $i = 0, ..., z_R$. Sodiation occurs when carboxylates on the protein surface bind Na^+, instead of protons, during the final stages of the CRM. Partial sodiation leads to mass heterogeneity and spreads the overall ion count over a range of adduct peaks, thereby reducing the signal-to-noise ratio (S/N) of the spectrum. The presence of other metal ion species will further degrade the spectral quality. Additional salt-induced signal suppression effects may be operational as well.[14]

Ammonium acetate is one of the few salts that is compatible with ESI-MS because it consists of two volatile components, i.e., ammonia and acetic acid. Like other cations, NH_4^+ associates with protein carboxylates as the droplet dries out. The resulting adduct then loses NH_3 during collisional activation in the ion sampling region of the mass spectrometer.

$$\begin{aligned} &\text{protein-COO}^- + \text{NH}_4^+ \\ &\rightarrow \text{protein-COO}^-\text{NH}_4^+ \\ &\rightarrow \text{protein-COOH} + \text{NH}_3 \end{aligned} \quad (3)$$

This two-step process generates a protonated carboxylic acid group, which contributes toward the formation of a clean $[M + z_R H]^{z_R+}$ signal.[6] NH_4^+ can even displace previously bound metal cations. To a certain extent, therefore, the presence of ammonium acetate can "rescue" ESI mass spectra of salt-contaminated samples.[43]

The discussion so far has not considered the presence of counterions in the solution. Droplet shrinkage during ESI, particularly during the final stage of the CRM, dramatically increases the concentration of any solute. These conditions favor nonspecific ion pairing. For example, when spraying proteins in the presence of NaCl, it is common to see analyte ions that are nonspecifically bound to both Na^+ and Cl^-. The resulting gaseous clusters have compositions $[M + (z_R - i)H + iNa + (NaCl)_j]^{z_R+}$ where both i and j can adopt a range of values. The heterogeneity caused by NaCl binding is yet another aspect that lowers the S/N of the spectrum.[44] The problem can be severe, because salts are often present in biological samples. Desalting by LC or microdialysis will improve the S/N under such conditions.[45]

Nonspecific binding can also affect ESI-MS studies on noncovalent protein−ligand complexes. In principle, native ESI-MS holds enormous promise for probing the nature of these biologically important interactions.[3] Transferring intact protein−ligand complexes into the gas phase for mass analysis can reveal binding stoichiometries. Under unfavorable conditions, however, the CRM gives rise to nonspecific adducts. Similar to cationization and salt adduction, nonspecific ligand binding can occur when chemical species that are trapped in the same nanodroplet start to interact as the solvent dries out. In these cases, ESI-MS reveals the presence of gas-phase complexes that do not exist in bulk solution. Strategies have been proposed to recognize and mitigate this problem.[9]

EJECTION OF NONPOLAR POLYMER CHAINS: THE CEM

The ESI behavior of a protein is governed by the chain conformation. In neutral aqueous solution, most proteins adopt a compact globular fold, where the majority of charged and polar residues point to the outside, maximizing favorable water interactions. Many nonpolar moieties are buried, forming a hydrophobic core that is not solvent accessible.[46] As discussed above, these native globular conformers follow the CRM.

MD simulations revealed that unfolded proteins undergo ESI via a different type of process, referred to as chain ejection model (CEM, Figure 5c).[19,47] Protein unfolding in solution can be triggered, e.g., by exposure to an acidic LC mobile phase. The resulting conformers are highly disordered, and nonpolar residues that were previously sequestered in the core are now solvent accessible. Thus, unfolding switches the properties of the protein from compact/hydrophilic to extended/hydrophobic.[48] This largely hydrophobic character makes it unfavorable for unfolded proteins to reside within the droplet interior. Instead, when placed in a Rayleigh-charged nanodroplet, unfolded chains immediately migrate to the droplet surface. One chain terminus then gets expelled into the vapor phase. This is followed by stepwise sequential ejection of the remaining protein and separation from the droplet. Clearly, the CEM has elements in common with the IEM (Figure 5a), whereas it is completely distinct from the CRM (Figure 5b). The CEM applies to polymer chains that are (i) disordered, (ii) partially hydrophobic, and (iii) capable of binding excess charge carriers.[19,20] MD data that illustrate the ejection of a protein model chain from a charged nanodroplet are depicted in Figure 6.

dx.doi.org/10.1021/ac302789c | Anal. Chem. 2013, 85, 2−9

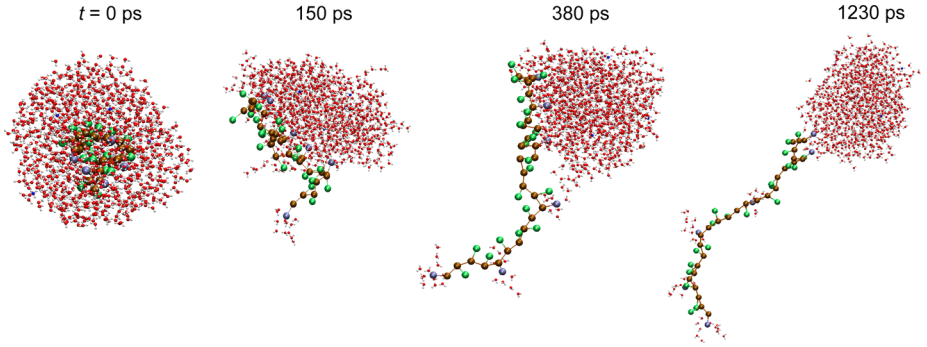

Figure 6. In this MD simulation, an unfolded protein chain that was initially placed within a Rayleigh-charged water droplet gets ejected via the CEM. Side chains and backbone moieties are represented as beads (brown: neutral backbone; green: neutral side chain; light blue: positive side chain; orange: negative side chain). Reprinted from ref 19. Copyright 2012 American Chemical Society.

PROTEIN SIGNAL INTENSITIES

Folded globular proteins tend to generate ESI mass spectra with relatively low intensities, whereas unfolded polypeptide chains provide more intense signals. For example, acid-induced unfolding enhances the total ion count of myoglobin by almost 2 orders of magnitude (Figure 7a,b). Much of this signal enhancement can be attributed to the different ionization mechanisms, i.e., CRM for native myoglobin and CEM for the unfolded protein. The CRM of a large globular analyte (Figure 5b) is a relatively slow and inefficient process that occurs on a μs time scale.[19,22,23] Hence, many folded protein molecules will remain nanodroplet-entrapped by the time they reach the interface region of the mass spectrometer. In contrast, the CEM leads to rapid (ns) ejection of unfolded/hydrophobic chains.[19,20] This high CEM rate enhances the ion yield and thus boosts the signal intensity of the unfolded chains.[19] It is noted, however, that other experimental parameters such as the transmission characteristics of the analyzer can also contribute to differences in signal intensity.[34]

PROTEIN CHARGE STATES

A variety of factors can modulate the ESI mass spectra of proteins, but the solution-phase conformation represents the main determinant of the observed charge state distribution.[49] Unfolded proteins show much higher charge states than their folded counterparts. For example, native myoglobin exhibits a narrow distribution centered at 9+ (Figure 7A). In contrast, the spectrum of the unfolded protein has its maximum shifted to 17+, and the charge state distribution is dramatically broadened (Figure 7b). Volatile acids are most commonly used for inducing solution-phase unfolding in ESI-MS, but high charge states are also observed after denaturation in base and cleavage of disulfide bridges, as well as for natively disordered proteins.[42,49] Numerous studies have exploited this effect for monitoring protein folding and unfolding in solution.[49]

The conformation-induced differences in ESI charge states are rooted in the different ionization mechanisms.[47] The low charge states of folded proteins are a consequence of the CRM, where the protonation behavior of the analyte is governed by eq 1 (see discussion above). For the myoglobin example of Figure 7a, the CRM predicts a charge state of z_R = 9.5. This matches the experimental data quite well.

The higher ESI charge states of unfolded proteins do not simply reflect the solution-phase titration state in solution.[14,49] Instead, highly protonated ions are formed as a result of charge equilibration during the CEM.[19,47] To understand the origin of this effect, we consider a closely related phenomenon, i.e., the dissociation of electrosprayed multiprotein complexes in the gas phase (Figure 5d). Slow collisional activation induces gradual unfolding of a single subunit. Driven by electrostatic repulsion, mobile protons on the surface of the complex spread into the subunit that is being unraveled (Figure 5d, middle panel). This charge transfer occurs up to the point where the subunit detaches. Ultimately, these events produce an unfolded protein that is highly charged and a residual complex that is charge-depleted.[50]

The dissociation processes of Figure 5d strongly resemble the ejection of an unfolded protein from a nanodroplet via the CEM (Figure 5c). In both cases, a Rayleigh-charged spherical moiety releases a highly protonated polymer chain. For the dissociation of multiprotein complexes, it is undisputed that the high charge state of the departing subunit originates from electrostatically driven proton transfer.[50] Analogously, it can be postulated that the high charge states generated during the CEM originate from proton equilibration between the highly charged ESI droplet and the protein that is being ejected (red arrows in Figure 5c,d).[19,47]

Finally, we address the fact that the ESI charge state distributions of unfolded proteins cover such a wide range of protonation states. The main contributor to this phenomenon appears to be ejection from Rayleigh-charged nanodropets with different radii. Under steady state conditions, an ESI source produces a range of droplet sizes.[6] Large droplets carry more charge than smaller ones (eq 1). More protons will therefore be imparted onto a protein that gets ejected from a larger droplet, whereas smaller droplets produce lower charge states (Figure 7c). The maximum droplet size capable of undergoing CEM[47] is around 10 nm, which defines the upper limit of the observed protein charge state range. In addition to the described droplet size effect, other factors may contribute to charge state heterogeneity is well. These include the presence of protein chains with different degrees of unfolding, incomplete charge equilibration during ejection, and the possibility that some chains get ejected below the Rayleigh limit. The charge equilibration/CEM concept summarized here can quantitatively account for experimentally observed ESI mass spectra of unfolded proteins.[47]

CONCLUDING REMARKS

The past few years have witnessed major advances in the general understanding of the ESI process. The IEM, CRM, and CEM provide a framework that is capable of accounting for a wide range of observations. Nonetheless, future work is needed

dx.doi.org/10.1021/ac302789c | Anal. Chem. 2013, 85, 2−9

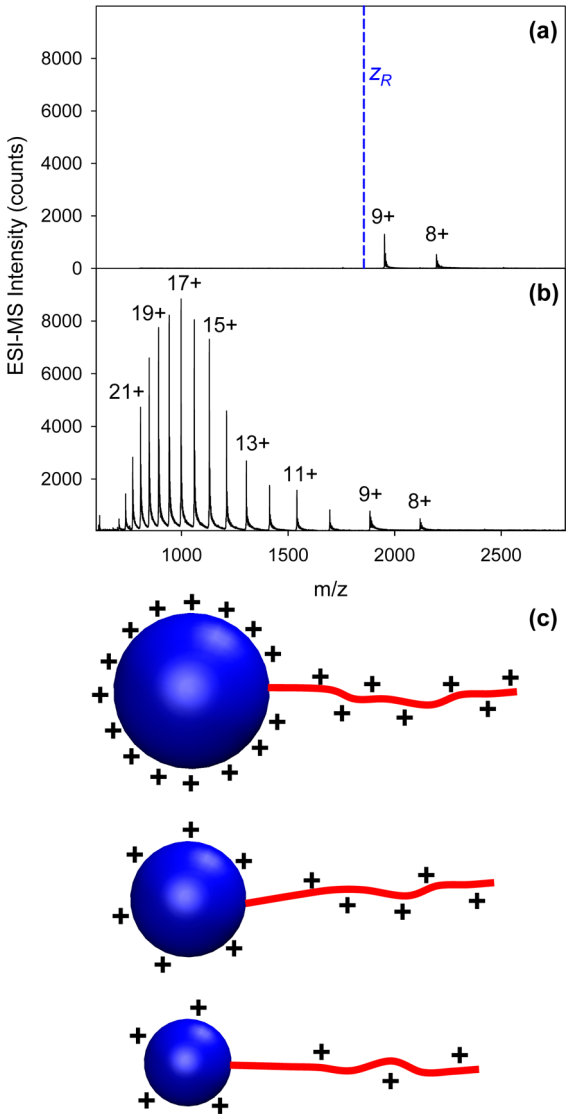

Figure 7. (a) ESI mass spectrum of native myoglobin at pH 7. The Rayleigh charge of z_R = 9.5 is indicated. (b) ESI mass spectrum of acid-unfolded myoglobin at pH 2. Except for pH, the conditions used for recording the two data sets were identical. The *y*-axes in (a) and (b) are scaled equally to emphasize the intensity difference. Protonation states are indicated as 9+, 11+, etc. (c) Schematic depiction of an unfolded protein (red) that separates from a charged nanodrolet (blue) during CEM. Large droplets produce protein ions that are more highly charged. Reprinted from ref 19. Copyright 2012 American Chemcial Society.

to further scrutinize the results and predictions obtained by these models. Numerous aspects remain to be uncovered, such as the question where exactly the dividing lines between the three ESI scenarios are located in terms of analyte size, structure, and polarity.[16] It is possible that additional ESI mechanisms will be discovered in the future. The current article exclusively focuses on the commonly used positive ion mode. Many of the general concepts outlined above should also apply to negative ion ESI, but this remains to be verified. Also, it will be interesting to explore whether the concepts summarized here can be adapted to the areas of ESI supercharging,[39] laser spray ionization (LSI),[51] desorption electrospray ionization (DESI),[52] and possibly even MALDI.[5] In any case, it is important for practitioners to acquire a mechanistic understanding of the ionization techniques used, as this will facilitate the design of experiments and the proper interpretation of data.

AUTHOR INFORMATION

Corresponding Author

*Telephone: (519) 661-2111 ext. 86313. E-mail: konerman@uwo.ca.

Notes

The authors declare no competing financial interest.

Biography

Lars Konermann is Professor of Chemistry and Canada Research Chair at The University of Western Ontario. The work of his group focuses on the development and application of novel MS techniques for biological applications. Major areas include the use of hydrogen/deuterium exchange and covalent labeling for exploring protein structure and dynamics. In addition, the research group has a broad interest in MS fundamentals. Elias Ahadi received his Ph.D. under Konermann's supervision in 2011. Ahadi developed molecular dynamics code and performed computer simulations for studying various aspects of the ESI process. Antony Rodriguez completed his B.Sc. in Chemistry and Biochemistry in 2012. For his graduate work in the Konermann laboratory, he studies protein–ligand interactions by hydrogen/deuterium exchange MS. Siavash Vahidi started his work in the Konermann group as a Ph.D. student in 2010. His research focuses on ultrarapid protein folding, as well as exploring the relationship between protein structure in solution and in the gas phase.

ACKNOWLEDGMENTS

Funding for this work was provided by the Natural Sciences and Engineering Research Council of Canada (NSERC), the Canada Foundation for Innovation (CFI), and the Canada Research Chairs Program.

REFERENCES

(1) Fenn, J. B. *Angew. Chem., Int. Ed.* **2003**, *42*, 3871.
(2) Karas, M.; Hillenkamp, F. *Anal. Chem.* **1988**, *60*, 2299.
(3) Heck, A. J. R.; Van den Heuvel, R. H. H. *Mass Spectrom. Rev.* **2004**, *23*, 368.
(4) Berkenkamp, S.; Kirpekar, F.; Hillenkamp, F. *Science* **1998**, *281*, 260.
(5) Knochenmuss, R. *Analyst* **2006**, *131*, 966.
(6) Kebarle, P.; Verkerk, U. H. *Mass Spectrom. Rev.* **2009**, *28*, 898.
(7) Nilsson, T.; Mann, M.; Aebersold, R.; Yates, J. R.; Bairoch, A.; Bergeron, J. J. M. *Nat. Methods* **2010**, *7*, 681.
(8) Percy, A. J.; Rey, M.; Burns, K. M.; Schriemer, D. C. *Anal. Chim. Acta* **2012**, *721*, 7.
(9) Kitova, E. N.; El-Hawiet, A.; Schnier, P. D.; Klassen, J. S. *J. Am. Soc. Mass Spectrom.* **2012**, *23*, 431.
(10) Liuni, P.; Jeganathan, A.; Wilson, D. J. *Angew. Chem.* **2012**, *51*, 9666.
(11) Marchese, R.; Grandori, R.; Carloni, R.; Raugei, S. *J. Am. Soc. Mass Spectrom.* **2012**, *23*, 1903.
(12) Hogan, C. J.; Carroll, J. A.; Rohrs, H. W.; Biswas, P.; Gross, M. L. *Anal. Chem.* **2009**, *81*, 369.
(13) de la Mora, F. J. *Anal. Chim. Acta* **2000**, *406*, 93.
(14) Cech, N. B.; Enke, C. G. *Mass Spectrom. Rev.* **2001**, *20*, 362.
(15) Van Berkel, G. J.; Kertesz, V. *Anal. Chem.* **2007**, *79*, 5511.
(16) Nguyen, S.; Fenn, J. B. *Proc. Natl. Acad. Sci. U.S.A.* **2007**, *104*, 1111.
(17) Ahadi, E.; Konermann, L. *J. Am. Chem. Soc.* **2010**, *132*, 11270.
(18) Ahadi, E.; Konermann, L. *J. Am. Chem. Soc.* **2011**, *133*, 9354.
(19) Ahadi, E.; Konermann, L. *J. Phys. Chem. B* **2012**, *116*, 104.
(20) Chung, J. K.; Consta, S. *J. Phys. Chem. B* **2012**, *116*, 5777.
(21) Daub, C. D.; Cann, N. M. *Anal. Chem.* **2011**, *83*, 8372.

(22) Patriksson, A.; Marklund, E.; van der Spoel, D. *Biochemistry* **2007**, *46*, 933.
(23) Steinberg, M. Z.; Breuker, K.; Elber, R.; Gerber, R. B. *Phys. Chem. Chem. Phys.* **2007**, *9*, 4690.
(24) Znamenskiy, V.; Marginean, I.; Vertes, A. *J. Phys. Chem. A* **2003**, *107*, 7406.
(25) Liuni, P.; Wilson, D. J. *Exp. Rev. Proteomics* **2011**, *8*, 197.
(26) Covey, T. R.; Thomson, B. A.; Schneider, B. B. *Mass Spectrom. Rev.* **2009**, *28*, 870.
(27) Wu, X.; Oleschuk, R. D.; Cann, N. M. *Analyst* **2012**, *137*, 4150.
(28) Van Berkel, G. J.; De La Mora, J. F.; Enke, C. G.; Cole, R. B.; Martinez-Sanchez, M.; Fenn, J. B. *J. Mass Spectrom.* **2000**, *35*, 939.
(29) Wang, R.; Zenobi, R. *J. Am. Soc. Mass Spectrom.* **2010**, *21*, 378.
(30) Rayleigh, L. *Philos. Mag.* **1882**, *14*, 184.
(31) Wilm, M.; Mann, M. *Anal. Chem.* **1996**, *68*, 1.
(32) Heemskerk, A. A. M.; Busnel, J. M.; Schoenmaker, B.; Derks, R. J. E.; Klychnikov, O.; Hensbergen, P. J.; Deelder, A. M.; Mayboroda, O. A. *Anal. Chem.* **2012**, *84*, 4552.
(33) Gibson, G. T. T.; Mugo, S. M.; Oleschuk, R. D. *Mass Spectrom. Rev.* **2009**, *28*, 918.
(34) Liu, J.; Konermann, L. *J. Am. Soc. Mass Spectrom.* **2011**, *22*, 408.
(35) Halliday, D.; Resnick, R.; Krane, K. S. *Physics*, 4 ed.; Wiley: New York, 1992.
(36) Iribarne, J. V.; Thomson, B. A. *J. Chem. Phys.* **1976**, *64*, 2287.
(37) Labowsky, M.; Fenn, J. B.; Fernandez de la Mora, J. *Anal. Chim. Acta* **2000**, *406*, 105.
(38) Gomez, A.; Tang, K. *Phys. Fluids* **1994**, *6*, 404.
(39) Iavarone, A. T.; Williams, E. R. *J. Am. Chem. Soc.* **2003**, *125*, 2319.
(40) Dole, M.; Mack, L. L.; Hines, R. L.; Mobley, R. C.; Ferguson, L. D.; Alice, M. B. *J. Chem. Phys.* **1968**, *49*, 2240.
(41) Kaltashov, I. A.; Mohimen, A. *Anal. Chem.* **2005**, *77*, 5370.
(42) Testa, L.; Brocca, S.; Grandori, R. *Anal. Chem.* **2011**, *83*, 6459.
(43) Iavarone, A. T.; Udekwu, O. A.; Williams, E. R. *Anal. Chem.* **2004**, *76*, 3944.
(44) Verkerk, U. H.; Kebarle, P. *J. Am. Soc. Mass Spectrom.* **2005**, *16*, 1325.
(45) Liu, C.; Wu, Q.; Harms, A. C.; Smith, R. D. *Anal. Chem.* **1996**, *68*, 3295.
(46) Fersht, A. R. *Structure and Mechanism in Protein Science*; W. H. Freeman & Co.: New York, 1999.
(47) Konermann, L.; Rodriguez, A. D.; Liu, J. *Anal. Chem.* **2012**, *84*, 6798.
(48) Creighton, T. E. *Proteins*; W. H. Freeman & Co: New York, 1993.
(49) Kaltashov, I. A.; Abzalimov, R. R. *J. Am. Soc. Mass Spectrom.* **2008**, *19*, 1239.
(50) Ruotolo, B. T.; Hyung, S.-J.; Robinson, P. M.; Giles, K.; Bateman, R. H.; Robinson, C. V. *Angew. Chem., Int. Ed.* **2007**, *46*, 8001.
(51) Trimpin, S.; Inutan, E. D.; Herath, T. N.; McEwen, C. N. *Mol. Cell. Proteomics* **2010**, *9*, 362.
(52) Cooks, R. G.; Ouyang, Z.; Takats, Z.; Wiseman, J. M. *Science* **2006**, *311*, 1566.